Dependence of CO2 advection patterns on wind direction on a gentle forested slope

B. Heinesch, Y. Yernaux, M. Aubinet

Biogeosciences, 5, 657–668, 2008
www.biogeosciences.net/5/657/2008/

Biogeosciences

Dependence of CO_2 advection patterns on wind direction on a gentle forested slope

B. Heinesch, Y. Yernaux, and M. Aubinet

Unité de Physique des Biosystèmes Faculté Universitaire des Sciences Agronomiques de Gembloux 8, avenue de la Faculté, B-5030 Gembloux, Belgium

Received: 19 October 2007 – Published in Biogeosciences Discuss.: 4 November 2007
Revised: 23 April 2008 – Accepted: 23 April 2008 – Published: 6 May 2008

Abstract. Gravitational flows generated on a gentle slope in stable conditions were analysed at a forested site at Vielsalm in Belgium. There were two distinct situations at the site, one corresponding to *vertical convergence*, characterised by a negative vertical velocity at the canopy top and horizontal velocity divergence below the canopy, the other corresponding to an *equilibrium* situation without any vertical movement. The causes of these two distinct flow patterns were analysed. These measurements combined with those of the horizontal CO_2 concentration gradient below the canopy supported the dilution hypothesis suggested by Aubinet et al. (2003): the horizontal CO_2 concentration gradient is negative in convergence situations but slightly positive in equilibrium conditions. The existence of such patterns allows us to confirm the coherence of advection observations made at the site. However, the sum of turbulent CO_2 flux, changes in CO_2 storage and advective terms were shown to greatly overestimate the expected net ecosystem exchange in the convergence conditions. The most probable cause was identified as being a poor estimate of the vertical profile of the vertical velocity component.

1 Introduction

Estimating the non-turbulent components of the CO_2 mass balance (horizontal and vertical advection, F_{HA} and F_{VA} respectively) has become a major challenge for micrometeorologists. These terms are assumed to be negligible over ideal flat and homogeneous terrain and under good turbulent mixing. The net ecosystem exchange (*NEE*) is then estimated by the sum of the vertical turbulent flux at the interface of the vegetation and the atmosphere (F_C) and the changes in CO_2 storage below this level (F_S). This method, referred as the eddy covariance technique, is clearly an invaluable tool for assessing biosphere-atmosphere exchange rates at the ecosystem scale and over the long term. However, concurrent with the multiplication of sites and the desire to measure above all kinds of ecosystems, a considerable number of sites are now situated in complex terrain. In these cases and especially under nocturnal conditions associated with weak winds, non-turbulent components of the mass balance can represent a non-negligible part of the *NEE*. Under these meteorological and topographical conditions, the sum F_C+F_S often fall short of the expected biological flux (Aubinet et al., 2000; Gu et al., 2005; Loescher et al., 2006). Many authors consider the non-turbulent fluxes as responsible for this underestimation (e.g. Froelich et al., 2005; Goulden et al., 2006; Knohl et al., 2003; ..Lee, 1998; Van Gorsel et al., 2007; Yi et al., 2005) despite the possibility that other mechanisms at work in the stable boundary-layer also play a role (see review by Aubinet, in press). In most cases, the physical mechanisms responsible for the CO_2 transport by the mean flow are identified as gravitational flows that appear when cold dense air is accelerated downslope by gravity or as breezes that appear when two different land surfaces, characterised by different radiation properties or heat capacities, warm or cool at different rates (Stull, 1988). However, only a few studies propose a direct evaluation of F_{HA} and F_{VA} in the presence of a gravitational flow or breeze (Aubinet et al., 2003; Feigenwinter et al., 2004; Feigenwinter et al., 2008; Leuning personal communication; Marcolla et al., 2005; Sun et al., 2007.; Staebler and Fitzjarrald, 2004) due to the high material and methodological effort needed to conduct such measurements. Moreover, the details of the mechanisms leading to advection are highly site-specific, depending on source distribution, topography and structure of the canopy. It is therefore necessary to understand and quantify advection processes at a variety of sites.

Correspondence to: B. Heinesch
(heinesch.b@fsagx.ac.be)

Published by Copernicus Publications on behalf of the European Geosciences Union.

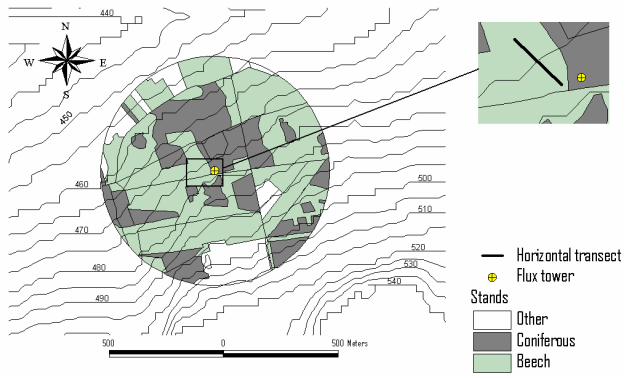

Fig. 1. Map of topography and land-use distribution around the flux tower; position of the horizontal transect and the main tower.

In this paper, we describe an intensive field experiment performed at a forested and gently sloping site at Vielsalm in Belgium with the aim of (i) describing the physical mechanisms responsible for advection and (ii) measuring advection to asses its importance in the CO_2 mass balance at the site. In section 2, we present the experimental set-up, details of the advection terms computation and the general characteristics of the flow pattern on the site. In Sect. 3, we describe two main gravitational flow patterns and their impact on the CO_2 concentration field. In Sect. 4, we compare all the terms of the CO_2 balance for these two main patterns, ending with our conclusions in Sect. 5.

2 Materials and methods

2.1 Site description

The study site is at Vielsalm in the Belgian Ardennes (50°18′N, 6°00′E, altitude 450 m), on the side of an open valley, with a uniform slope oriented NW with a 3% incline (1.7°). The climate is temperate maritime. The stand is mixed, comprising Douglas fir (*Pseudotsuga menziesii* [Mirb.] Franco), beech (*Fagus sylvatica* L.), silver fir (*Abies alba* Miller), Norway spruce (*Picea abies* [L.] Karst.), Scots pine (*Pinus sylvestris* L.) and pedonculate oak (*Quercus robur* L.). The tower is at the interface of two sub-plots, one sub-plot dominated by Douglas fir, 36 m maximum height, 112 $m^2\,ha^{-1}$ basal area, 49 stems ha^{-1} with very sparse undercover, and the other dominated by beech, 27 m maximum height, 129 $m^2\,ha^{-1}$ basal area, 145 stems ha^{-1} with no undercover. The distance to the forest edge is 1 500 m and 500 m respectively , to the SW and the NE (the dominant synoptic wind directions). A clearing with a 5-ha tree nursery is 250 m away from the tower in the upslope direction (Fig. 1). The vegetation area index (VAI), deduced from photosynthetically active radiation measurements above and below the canopy (transect of height sensors) was estimated to be close to 5 for both subplots, despite different canopy architectures. The soil at the site is 100–150 cm deep and is classified as dystric cambisol. A more complete description of the site can be found in Laitat et al. (1999); the site was part of the successive Euroflux, CarboEuroflux and CarboEurope networks.

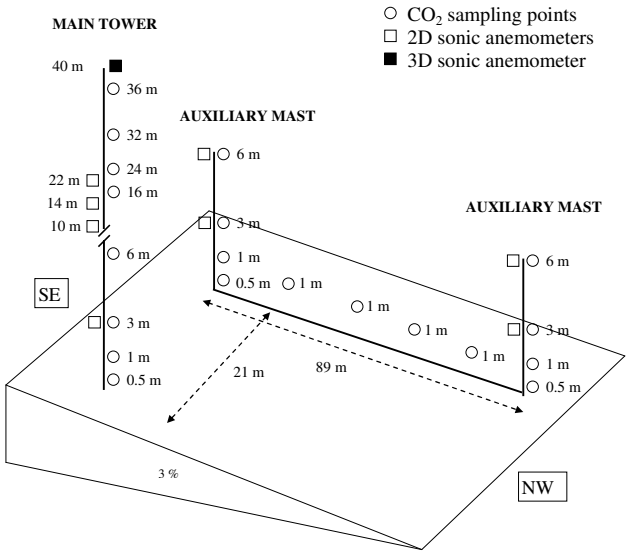

Fig. 2. Schematic representation of the experimental setup.

3 Experimental set-up

A detailed description of the long-term flux measurement system, including the eddy covariance system and the micrometeorological station, was given by Aubinet et al. (2001). In addition to this set-up, a system devised to estimate the advection terms was installed for four months in summer 2002 in the beech sub-plot. It measured the CO_2 concentration of the air and the horizontal velocity at several points below the eddy covariance sensor. The three-dimensional sonic anemometer (Gill R2, Gill Instruments, Lymington, UK) of the eddy covariance system was used to estimate the vertical component of the velocity above the forest, and was placed at the top of the main tower, at a height of 40 m, fixed on a vertical boom 4 m long. Half-hourly averages of the air CO_2 concentrations were measured at 20 points (Fig. 2). Three vertical profiles were taken, two of them on two secondary masts situated 89 m from each other along the slope direction, with four sampling heights (0.5, 1, 3 and 6 m), and the third one at the main tower, not aligned with the two secondary masts, with eight sampling heights (0.5, 1, 3, 6, 16, 24, 32 and 36 m). In addition, one horizontal profile with four sampling points, each of them at 1 m above ground level, was taken between the two secondary masts. These points were evenly distributed along the transect. The total cycling time through these 20 inlet points was 3 min 40 s. The lines were sampled one by one using a

pump (KNF N86KN18) but air was flushed constantly along all the lines (with two more identical pumps) in order to reduce the total cycling time. The response time of the system (i.e., the time needed to purge the flow path downstream from the valve selecting the sampling line of air coming from a previous sampling point) was evaluated to be shorter than 3 s. Therefore, after line switching, a delay time of 4 s was imposed before recording data. After this delay time, five consecutive samples were taken at a frequency of 0.7 Hz. Finally, each concentration measurement corresponded to an average of eight periods with five samples each, taken at uniform frequency over the half-hour period. All concentrations were measured using the same infrared gas analyser (model LI-6262 with pressure transducer, LI-COR Inc., Lincoln, NE, USA). Horizontal velocity was measured at four heights (3, 10, 14 and 22 m) on the main tower using homemade sonic anemometers pointing in the SE direction to avoid flow distortion by the tower in conditions of downslope flows below the canopy. These anemometers were calibrated by comparison with a Gill R2 anemometer and they performed well for low mean wind velocities. During the experiment, two similar anemometers were added to each secondary mast (at heights of 3 and 6 m, Fig. 2) in order to estimate the divergence of the horizontal velocity. The divergence analysis was restricted to close alignment of the near ground wind on the slope transect. The 3 and 6 m levels gave similar results, indicating that the sonic anemometers performed well. More technical details on the tubing, the $[CO_2]$ sampling sequence and the home-made sonic anemometers can be found in Heinesch et al. (2007).

4 CO_2 budget

The carbon dioxide conservation equation states that the CO_2 produced or absorbed by the biological source/sink is either stored in the air or removed by flux divergence in all directions. This equation has been developed and discussed in detail, notably by Baldocchi et al. (1988). After applying Reynolds decomposition, spatial integration over a control volume of height h and lateral extent $2L$, neglecting the horizontal turbulent flux divergence and the horizontal variation of the vertical turbulent flux, the equation is reduced to:

$$NEE = \frac{1}{V_m}\left[\int_0^h \left[\frac{\partial \bar{c}}{\partial t}\right] dz + \left(\overline{w'c'}\right)_h + \int_0^h \bar{w}(z)\frac{\partial \bar{c}}{\partial z}dz + \frac{1}{4L^2}\int_{-L}^{+L}\int_{-L}^{+L}\int_0^h \left(\bar{u}\frac{\partial \bar{c}}{\partial x} + \bar{v}\frac{\partial \bar{c}}{\partial y}\right) dxdydz\right] \quad (1)$$

where *NEE* (in μmol m^{-2} s^{-1}) represents the sum of the vertically integrated canopy source/sink term and the diffusional CO_2 flux emanating from the soil, c is the CO_2 mixing ratio (in μmol mol^{-1}) defined as the ratio of mole density of CO_2 to the mole density of dry air, V_m is the molar volume of dry air (m^3 mol^{-1}) and u, v and w represent the velocity components, respectively in the horizontal (x, y) and vertical (z) directions. Overbars represent time averages (used here for short-term time averages; i.e. 30 min) and primes departures therefrom. The four terms on the right-hand side represent, respectively, the rate of change in storage in the air of the control volume (F_S), the vertical turbulent transport (F_c), the vertical advection (F_{VA}) and the horizontal advection (F_{HA}) of CO_2. The sign convention for all the transport terms (F_c, F_{VA} and F_{HA}) is that positive values refer to a transport of CO_2 out of the control volume. Positive storage flux represents an additional source of carbon; negative refers to a carbon sink in the control volume. Lateral integration has already been performed on the first three terms on the right-hand side by assuming that they do not vary in the x and y directions. The upper boundary of the box is in the air at the height of the eddy covariance measurement system (h).

If, for the sake of simplicity, lateral homogeneity is assumed (see next section for the justification of this hypothesis at our site) the volume will be restricted to a two-dimensional (2-D) box along the x and z axes and F_{HA} may be written:

$$F_{HA} = \frac{1}{2L}\frac{1}{V_m}\int_{-L}^{L}\int_0^h \bar{u}\frac{\partial \bar{c}}{\partial x}dxdz = \frac{1}{V_m}\int_0^h \bar{u}_{x=0}(z)\frac{\bar{c}_{x=+L}(z) - \bar{c}_{x=-L}(z)}{2L}dz = \frac{1}{V_m}\int_0^h \bar{u}_0(z)\frac{\Delta \bar{c}(z)}{2L}dz \quad (2)$$

where the horizontal integration is performed by assuming a horizontally homogeneous horizontal gradient ($\partial^2\bar{c}/\partial^2 x$)=0 and horizontal velocity divergence (($\partial^2\bar{u}/\partial^2 x$)=0). The x axis is oriented downslope and thus a positive (negative) horizontal $[CO_2]$ gradient reflects an enrichment (depletion) of the air in CO_2 when flowing downslope. An uncertainty analysis of F_{VA} and F_{HA} was presented by Heinesch et al. (2007).

5 Flow pattern description

Previous studies have already investigated the flow and $[CO_2]$ field pattern during the night, at the Vielsalm site (Aubinet et al., 2003, 2005; Heinesch et al., 2007). The wind directions above the canopy were mainly SW or NE. Despite the existence of a well defined slope, the valley is quite open and it's likely that the flow above the canopy is not influenced by the topography but is rather driven by synoptic conditions, representative of the entire region. In unstable and neutral atmospheric conditions, resultant wind vectors above and below the canopy corresponded fairly closely, indicating a good coupling between the above and below canopy wind regimes, and a limited impact of the directional wind shear on the site. In contrast, under stable conditions, the wind regime near the ground was dominated by downslope air movements that

showed little coupling with the flow aloft. This decoupling in wind directions was easy to observe because the site presents the particularity of having the local slope direction (SE to NW) perpendicular to the main wind directions above the canopy. As the stable conditions were also shown to coincide with the underestimation of the *NEE*, defined as the sum of the turbulent eddy flux and the storage, the gravitational flows were considered to be responsible for the additional CO_2 transport not accounted for by the flux measurement system. This specific air movement occurred on stable nights characterised by strongly negative net radiation. The gravitational layer was shown to be limited to about half the canopy height with a wind that was well aligned with the slope direction. Under these conditions, the [CO_2] evolution along a streamline was shown to be quite regular and reproducible from one streamline to another at the same height (Heinesch et al., 2007). This, combined with the rather monoclinic site topography in the main tower surroundings, justifies the limitation of the set-up to a 2-D framework. During these gravitational flow events, a qualitative evaluation of the advection terms showed that F_{VA} was positive and F_{HA} was negative under stable conditions (Aubinet et al., 2003). A quantitative evaluation of F_{VA} and F_{HA} was difficult because the experimental set-up at that time was too crude. In this study, we will restrict ourselves to situations of gravitational flows. In these conditions, our 2-D set-up has the ability to estimate the horizontal [CO_2] gradient along a streamline in the gravitational layer, which is a mandatory variable for estimating F_{HA}, and the divergence of the horizontal wind speed along a streamline which will be useful to distinguish different gravitational flow patterns and to constrain the vertical profile of $\bar{w}$ (see Sects. 3 and 4). In the following discussions, we will focus on periods when the mechanisms driving the gravitational flows were well established. This was done by selecting gravitational flow events lasting at least several consecutive half-hours. Using the threshold of three consecutive half-hours, 50 events (representing 652 half-hours) were selected over 106 nights available in the dataset. Gravitational flow events were detected through visual inspection of the wind direction above the canopy and in the trunk space: a half-hour presenting a wind-direction in the trunk-space from the SE quadrant ($\pm 45°$ of the slope direction) while the wind above the canopy was blowing from another quadrant was considered as showing gravitational flow events. This wind-direction selection criteria was shown to be closely related to the stability parameter or to strongly negative net radiation, as already stated, but more restrictive than them. This filtering of gravitational flow events based on wind directions was applicable for Vielsalm because the orientation of the local slope is very different from the wind directions aloft. For sites which do not present such a particular situation, the identification of the gravitational events could be done by analysing the relative importance of the driving forces acting on the flow near the ground following for example the study of subcanopy flows made by Staebler and Fitzjarrald (2005).

6 Vertical integration of advection terms

The computation of F_{HA} and F_{VA} requires a vertical integration on the whole height of the control volume. As vertical profiles of c and u are discrete and do not cover the whole height, they should be interpolated and extrapolated before the integration. To do that, we postulate that, during the gravitational flow events, the spatial and temporal dependencies of the vertical profiles of u and Δc can be separated (i.e. the normalized vertical profiles are assumed to be constant with time):

$$\begin{aligned} \Delta\bar{c}\,(t,z) &= \Delta\bar{c}_{\mathrm{ref}}\,(t)\,f(z) \\ \bar{u}\,(t,z) &= \bar{u}_{\mathrm{ref}}\,(t)\,g(z) \end{aligned} \tag{3}$$

where $\Delta\bar{c}_{\mathrm{ref}}(t)$ and $\bar{u}_{\mathrm{ref}}(t)$ are respectively the horizontal concentration difference and the horizontal component of the wind speed at a reference level and the functions $f(z)$ and $g(z)$ are profile functions that are assumed to be independent of time. $f(z)$ and $g(z)$ were parameterised using an exponential and a beta function respectively:

$$\begin{aligned} f(z) &= e^{-(z-z_{\mathrm{ref}})/k} \\ g(z) &= a_{0\mathrm{mean}} z^{a_{1\mathrm{mean}}} (20-z)^{a_{2\mathrm{mean}}} \end{aligned} \tag{4}$$

where $k, a_{0\mathrm{mean}}, a_{1\mathrm{mean}}, a_{2\mathrm{mean}}$ are adjustable parameters obtained by least square fitting (k=5.23 m, $a_{0\mathrm{mean}} = 0.039\mathrm{m}^{-1.403}$, $a_{1\mathrm{mean}}$=0.454, $a_{2\mathrm{mean}}$=0.949) and z_{ref} is the reference height used for the normalization of the profile functions. This choice was driven by the observed shapes of the measured profiles. The exponential decrease for f reflects the behaviour of the measured profile of concentration difference in the trunk space well and a Beta function for g is able to reproduce the secondary maximum of wind speed in the trunk space (Fig. 3). It's worth noting that the expression for $\bar{u}$ in Eq. 3 does not take into account the divergence of $\bar{u}$ along the slope that would be associated with a vertical air movement. However, the quantitative impact of this approximation on F_{HA} will be small because $\bar{u}$ is multiplied by a small horizontal concentration difference. The adjustment of the profile functions was done on a selected dataset, corresponding to wind above the canopy blowing from the NE sector. We will show later (in Sect. 3) that the vertical concentration profile is more pronounced in these conditions. These functions were then used for all the gravitational flow events dataset.

Through the choice of the g function, we limited the vertical integration to 20 m, approximately the trunk space and the depth of the gravitational flow. This point will be discussed later. Moreover, the Beta function clearly underestimated $\bar{u}$ at the top of the gravitational layer. This had, however, very little impact on F_{HA} because the horizontal concentration gradient is weak in the upper part of the profile. Even if it cannot be confirmed by measurements, this is very likely because the main CO_2 sources are concentrated

close to the ground and because horizontal advection is believed to be restricted to the gravitational layer. Another potential limitation of this fit is the difficulty to reproduce the exact position of the maximum in wind speed. Refinement of the wind profile could be achieve with a parameterization of the wind profile in conditions of gravitational flows over a forested slope, something which has been done by Yi et al. (2005) but that requires unavailable detailed information about the vertical structure of the canopy. The sensitivity of the resulting F_{HA} to the profile function choice will be tested later.

The horizontal advection term is then computed, each half-hour, as:

$$F_{HA} = \frac{1}{V_m}\frac{1}{2L}\overline{u}_{0\mathrm{ref}}(t)\Delta\bar{c}_{\mathrm{ref}}(t)\int_0^h [g(z)f(z)]dz$$
$$= \frac{1}{V_m}\frac{1}{2L}\overline{u}_{0\mathrm{ref}}(t)\Delta\bar{c}_{\mathrm{ref}}(t)hS_{fg}, \quad (5)$$

where S_{fg} is a constant shape factor resulting from the integration of the profile function product. The reference heights were chosen to be 1 m for the concentrations and 3 m for the horizontal wind speed. As more than two measurements were available for the 1 m concentration evolution along the streamlines, $\Delta\bar{c}_{\mathrm{ref}}$ was deduced each half-hour by linear regression on the six measurements evenly distributed along the horizontal transect.

The normalized vertical profile of net transport by horizontal advection, calculated as the product of the two profile functions f and g, is presented in Fig. 3. The net transport is maximal at 2 m above ground level and the shape factor then equalled 0.13 at our site. This result is very similar to that given by Staebler and Fitzjarrald (2004) who found in the Harvard forest a marked maximum of transport only at 1 m above ground level. The sensitivity of this shape factor (and thus of F_{HA}) to the profile function choice and to the fitting parameters has been tested. Indeed, S_{fg} was recomputed with the mean value of $k\pm$ its standard error (5.23±0.56 m). The uncertainty related to the value of the parameter k induces a relative uncertainty on S_{fg} of 10% showing that the huge dispersion of the horizontal [CO_2] differences has only a restricted impact on F_{HA}. For g, we tested the replacement of a Beta function by a more simpler double linear regression (the first between 0 and 3 m using these measurements and the other between 3 and 20 m using measurements at levels 3, 10 and 14 m). This alternative choice for g has a relative impact on S_{fg} of only 15%, showing that a wrong representation of the wind profile in the upper part of the gravitational layer has only a limited impact on F_{HA} because the f function is close to zero in this layer.

To perform the vertical integration of F_{VA}, we will postulate, following Lee (1998), a linear vertical profile of the vertical velocity component. With this hypothesis, the term F_{VA} can be rewritten as:

$$F_{VA} = \frac{1}{V_m}\bar{w}_h.(\bar{c}(h) - \langle\bar{c}\rangle), \quad (6)$$

where $\bar{w}_h$ is the wind component above the canopy corrected for sensor tilt, flow distortion and instrumental offset using the method described in Lee et al. (2004, chapter 3) and $\langle\bar{c}\rangle$ is the mean [CO_2] between the soil and the height h. The arbitrary choice of a linear $\bar{w}$ vertical profile, often made in the literature, can have an important numerical impact on the computation of F_{VA} and will be discussed in Sect. 4.2.

Finally, F_{HA} was computed in the layer 0–20 m while F_{VA} was computed on the whole 40 m layer. This choice was imposed by experimental set-up limitations and will be discussed later.

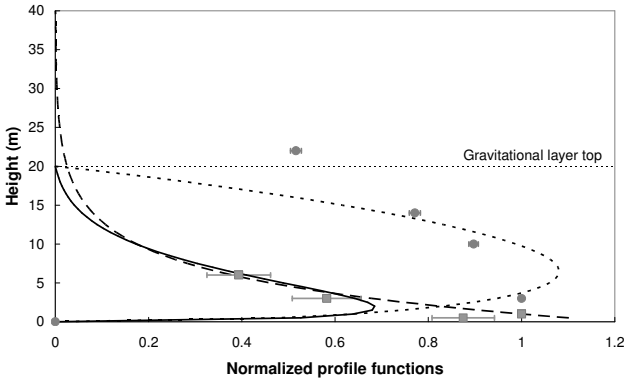

Fig. 3. Vertical profile functions $f(z)$ (dashed line) and $g(z)$ (dotted line) and their product $f(z)g(z)$ (solid line). The points (circles for $\Delta\bar{c}$ and squares for $\bar{u}$) represent the measurements at different levels normalized by the value at the reference level (1 m for f and 3 m for g). Error bars represent standard error of the mean. Established for periods with gravitational flows in the trunk space and NE ambient wind direction.

7 Link between flow and CO_2 concentration fields

7.1 Results

Figure 4 presents the evolution with the ambient wind direction of the vertical wind velocity component above the canopy ($\bar{w}_{40\,m}$) for the selected gravitational flow events. It is clearly negative when ambient wind is blowing from the sector 0–150°, and close to zero elsewhere. This suggests that, under stable conditions, two types of gravitational flows may occur, one with a negative vertical wind velocity, the other without. As the first category is associated with ambient wind from the 0–150° sector, it will be designated as the "NE sector". Similarly, the second category will be designated as the 'SW sector' because SW is the most frequent wind direction in the remaining data. In the following figures, all the relationships will be presented separately for the

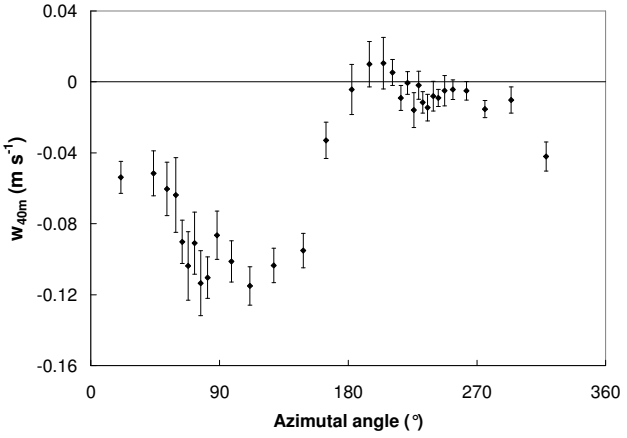

Fig. 4. Mean and standard error of the rotated vertical velocity component above the canopy ($\bar{w}_h$) as a function of the incoming ambient wind direction for the selected gravitational flow events. Each point corresponds to a mean on 20 half-hours.

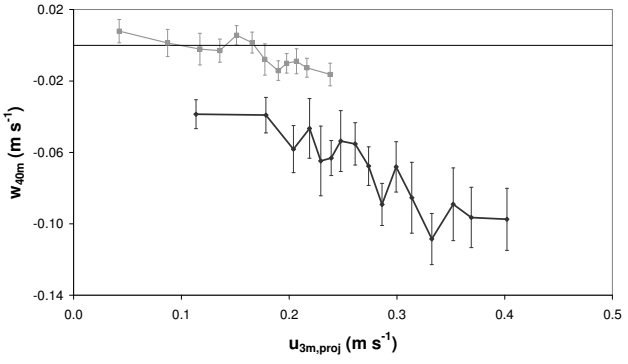

Fig. 5. Mean and standard error of the vertical velocity at 40 m as a function of the horizontal velocity 3 m above ground level projected on the slope direction. Established for periods with gravitational flows in the trunk space and for two ambient wind sectors (black: NE sector; grey: SW sector). Each point corresponds to a mean on 20 half-hours.

NE and SW sectors, data relating to the NE (SW) sector being represented in black (grey). These two sectors present similar mean horizontal wind speeds of about 1 m s^{-1} in stable conditions. However, it is worth noting that the two sectors present differences in land cover, the NE sector being planted mainly with Douglas fir and the SW sector with beech. The potential implications on the flow field will be discussed below.

The evolution of $\bar{w}_{40\,m}$ with the projection in the slope direction of horizontal velocity in the trunk space ($\bar{u}_{3\,m,\mathrm{proj}}$) is given for each sector in Fig. 5. It is clear, in the first instance, that the evolutions of $\bar{w}_h$ with $\bar{u}_{3\,m,\mathrm{proj}}$ are very different between the two sectors: in the NE sector, $\bar{w}_h$ increases with $\bar{u}_{3\,m,\mathrm{proj}}$ reaching absolute values up to 10 cm s^{-1}, while in the SW sector, $\bar{w}_h$ is very weak, below 2 cm s^{-1}, and only

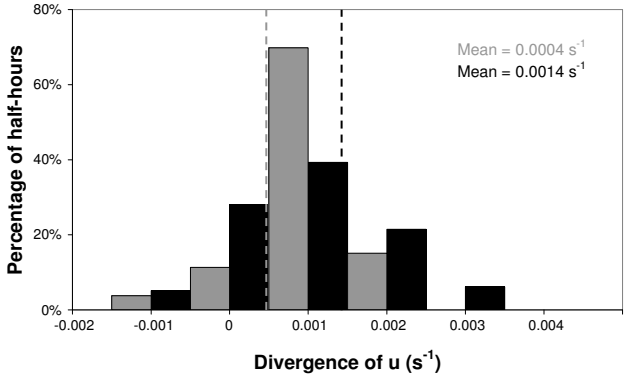

Fig. 6. Frequency distribution of along-slope wind speed horizontal divergence in the trunk space for periods with gravitational flows in the trunk space (black: NE sector; grey: SW sector). Mean of two levels of measurement (3 m and 6 m).

weakly depends on the velocity in the trunk space. In addition, the range of projected horizontal velocity is greater in the NE than in the SW sector. Indeed, $\bar{u}_{3\,m,\mathrm{proj}}$ varies between 11 and 40 cm s^{-1} with a mean of 27 cm s^{-1} in the former and between 4 and 23 cm s^{-1} with a mean of 16 cm s^{-1} in the latter. Finally, the horizontal divergence of these velocities in the trunk space also differs between the sectors, being more than three times higher in the NE (0.0015 s^{-1}) than in the SW (0.0004 s^{-1}) sector (Fig. 6). For the divergence analysis, it's worth noting that in order to make the calculation of the divergence more justifiable, the dataset had been filtered to keep only data showing close alignement of the near-ground wind with the slope transect. After filtering, 38% of the initial dataset is left and we postulate that this subset is representative of the whole dataset.

Vertical profiles of potential temperature (θ) relative to the top of the canopy obtained on the main tower are presented for each sector in Fig. 7. Here again, only measurements obtained under gravitational flow events were selected. In addition, only clear sky conditions (net radiation below – 50 W m^{-2}) were retained in order to ensure that the differences between the sectors were not due to a difference in radiation regime. The total vertical gradient was always negative, producing a thermal inversion in the forest despite the closed canopy ($VAI \cong 5$). The main difference between the sectors appears below 20 m where a thermal inversion of 0.5°C appears in the NE sector while no gradient is observed in the SW sector. This zone corresponds to the trunk space where most of the gravitational flow extends under stable conditions. The presence of a vertical potential temperature gradient in this layer is thus linked to the development of the gravitational flow.

Finally, the evolution with stability of the along-slope horizontal CO_2 concentration difference at 1 m above ground level is presented for the two sectors in Fig. 8. In the NE

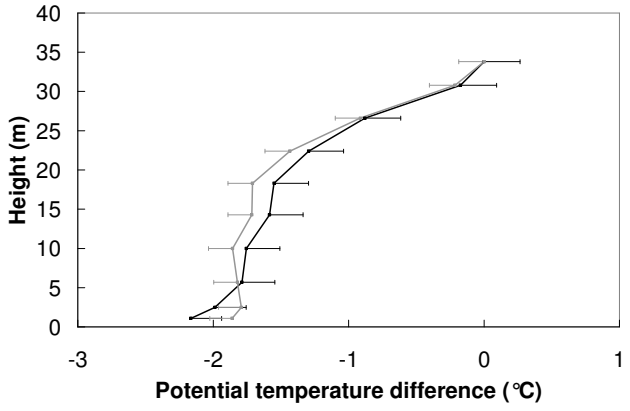

Fig. 7. Vertical profile of potential air temperature relative to 34 m in conditions of gravitational flows and under a clear sky (net radiation below –50 Wm^{-2}). Established for two ambient wind sectors (black: NE sector; grey: SW sector). Each point corresponds to a mean of 213 (104) half-hours. Error bars represent standard error of the mean.

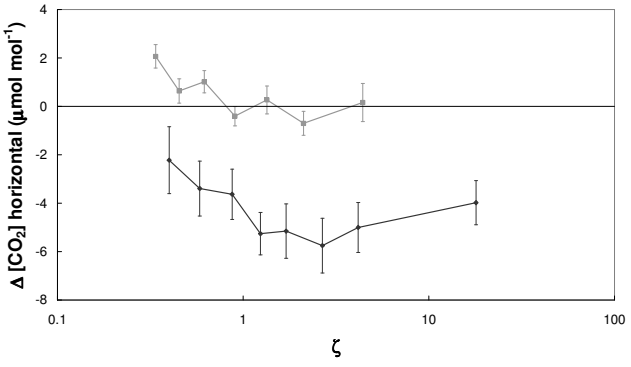

Fig. 8. Evolution with stability of the along slope [CO_2] difference at 1 m above ground level in conditions of gravitational flows. Established for two ambient wind sectors (black: NE sector; grey: SW sector). Each point corresponds to a mean of 50 half-hours. Error bars represent standard error of the mean.

sector, it is negative and increases in absolute value with increasing stability, reaching up to –6 μmol mol^{-1} (equivalent to a gradient of 0.067 μmol mol^{-1} m^{-1}) under very stable conditions. In the SW sector, it is slightly positive under moderately stable conditions and zero under strongly stable conditions.

8 Discussion

These results allow the processes at work in the canopy during periods with gravitational flows to be described more precisely. The two situations are represented schematically in Fig. 9. The more pronounced potential temperature vertical profile in the NE than in the SW sector suggests a more important action of buoyancy forces. This could explain not

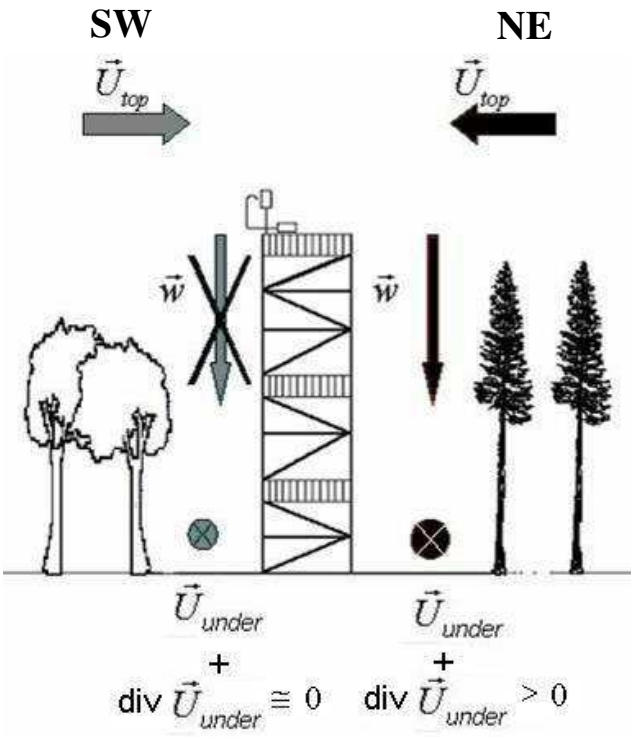

Fig. 9. Schematic representation of the two types of general flow patterns above and in the forest in nocturnal stable conditions. The slope direction is perpendicular to the sheet and inward.

only the larger surface velocity but also the larger horizontal velocity divergence observed in this sector. In addition, the larger horizontal velocity divergence is consistent with the larger vertical velocity in the NE sector, by the continuity equation. The situation observed in the NE sector therefore corresponds clearly to a vertical convergence situation described by Aubinet (in press).

Mahrt (1982) evaluated the horizontal wind speed in gravitational flow as $\bar{u}(x)=(\frac{g\Delta\bar{\theta}}{\bar{\theta}}L\sin\alpha)^{\frac{1}{2}}$ when only the buoyancy forces intervene in the momentum equation. Taking into account the results in Fig. 7 ($\Delta\theta$=0.5 K, θ=285 K) and the topographic characteristics of the site (L=300 m, α=1.7°), the wind speed is estimated to 0.4 m s^{-1} for the NE sector, which corresponds to the maximum observed values. This estimate accords well with our results considering that the terms describing the braking of the gravitational flow (entrainment, pressure gradients along the slope, drag forces) were not taken into account in this expression.

In contrast, in the SW sector the vertical profile of potential temperature is almost flat in the trunk space suggesting a lower importance of the local buoyant forces which is confirmed by the smaller surface wind horizontal divergence. However, the surface velocity is not zero, suggesting dominant buoyancy forces upstream that could provoke a lower but significant flow. Above canopy vertical velocity and near

ground velocity divergence measurements are also consistent, both being very small in these conditions. This situation corresponds to an equilibrium situation described by Aubinet (in press).

This suggests in synthesis that, according to the values of the various forces in action, the gravitational flow could be accelerated (horizontal divergence and vertical convergence) or maintained at a constant speed (equilibrium).

The impact of the flow pattern on the CO_2 concentration field was also clear. In the case of vertical convergence, a negative horizontal gradient was observed while in case of equilibrium the gradient was close to zero. Both gradient signs are possible in presence of vertical movements. On the one hand, as the air coming from the top is poorer in CO_2 than the air circulating in the gravitational flow layer, it helps to dilute the CO_2. On the other hand, the contribution due to soil respiration helps increase the concentration along the streamline. In general, the sign of the horizontal [CO_2] gradient will depend on the balance between these two terms. Using a simple model based on the continuity equation, Aubinet et al. (2005) showed that it ultimately depended on the source distribution upstream of the control volume. According to this model, the presence of a negative sign in NE conditions at Vielsalm would suggest that CO_2 sources are stronger upstream than in the control volume. This should be checked experimentally. In the case of equilibrium pattern (SW sector), the same model predicts that the horizontal gradient should be positive, and that is observed in moderately stable conditions.

It is not completely clear, however, why these particular situations are associated with wind direction or what the cause is of the downward vertical movement in the NE sector. As local buoyancy associated with continuity equation can be invoked as described above, the impact of a pressure gradient due to land cover heterogeneity could also be invoked. Indeed, due to the smaller tree height in the beech sub-plot than in the Douglas sub-plot, it is possible that streamlines above the canopy would be deflected downward when wind blows from the NE sector, eventually creating a rotor behind the height transition. However, this effect alone does not explain the presence of a negative temperature gradient in the lower layer. In addition, the close link between the vertical velocity above the canopy and the horizontal CO_2 gradient at 1m above the ground suggests that when a downward air movement above the canopy is detected, this air penetrates into the forest and at least of part of it goes down close to the soil. Finally, because tilt corrections, established with strong wind conditions only, have been applied to the velocity components, the velocity component discussed here is the one perpendicular to the long-term, strong winds streamlines. It means that negative vertical velocities for the NE sector in stable conditions are produced by a mechanism specific to stable conditions, which reduces the possibility of a major contribution from a rotor due to the height differences of the two subplots.

9 CO_2 budget including advective transport terms

9.1 Results

Equations 5 and 6 show that the four variables required to estimate the advection are $\bar{u}_{0\mathrm{ref}}$, $\Delta\bar{c}_{\mathrm{ref}}$,$\bar{w}_h$ and $\bar{c}(h)-\langle\bar{c}\rangle$. The mean nocturnal evolutions of $\bar{u}_{0\mathrm{ref}}$ and $\Delta\bar{c}_{\mathrm{ref}}$ are given in Fig. 10a and b for the NE and SW sectors, respectively and the mean nocturnal evolutions of $\bar{w}_h$ and $\bar{c}(h)-\langle\bar{c}\rangle$ are given in Fig. 10c and d for the NE and SW sectors, respectively. Only data collected under gravitational flow events were selected. Periods for which the amount of data was insufficient (less than 10 values) were removed which explains the absence of data in the transitional periods (beginning and end of the night).

In the NE sector, as noted earlier, $\bar{u}_{0\mathrm{ref}}$ is larger than in the SW sector (Fig. 10a and b). This variable remains constant during the night and does not vary significantly from night to night, confirming the consistence and repeatability of the flow pattern at the site in stable conditions. $\Delta\bar{c}_{\mathrm{ref}}$ is higher in absolute values in the NE than the SW sector (–3 μmol mol^{-1} against –0.2 μmol mol^{-1}), with an important night-to-night variability and no significant temporal trend during the course of the night. As a result, the horizontal advection is negative and non-negligible in the NE sector (between 0 and –2 μmol m^{-2} s^{-1}, mean=–1.2 μmol m^{-2} s^{-1}) and close to zero in the SW sector (mean=–0.2 μmol m^{-2} s^{-1}, Fig. 11c and d).

$\bar{w}_h$ time evolution also clearly differs between the two sectors, decreasing from –0.05 to –0.10 m s^{-1} in the NE sector (Fig. 10c) and being not significantly different from zero in the SW sector (Fig. 10d). The increase in absolute values of $\bar{w}_h$ with time in the NE sector suggests that the vertical movement establishes itself progressively during the night. No important differences in $\bar{c}(h)-\langle\bar{c}\rangle$ were observed between the sectors: they were both negative and between –5 and –8 μmol mol^{-1}. As a result, vertical advection was very different between the sectors, ranging from 5 to 30 μmol m^{-2} s^{-1} for the NE sector and between –5 and 5 μmol m^{-2} s^{-1} for the SW sector.

These results allow all the terms of the CO_2 balance to be evaluated. The nocturnal evolution of the five terms in Eq. (1) is presented in Fig. 11. The *NEE* was deduced by a simple empirical soil temperature model calibrated using turbulent and storage measurements selected at high values of friction velocities. It varied between 4 and 5 μmol m^{-2} s^{-1} and did not show any nocturnal trend.

In the NE sector, the sum of storage and turbulent terms presents a clear temporal evolution: it is close to the *NEE* in the early evening, due to important storage, and then decreases gradually. Such evolution was not observed in the SW sector but this could be because the night beginning was not represented because of an insufficient amount of data. We will discuss this further below. This shows that the sum of storage and turbulent terms is always lower than the *NEE*,

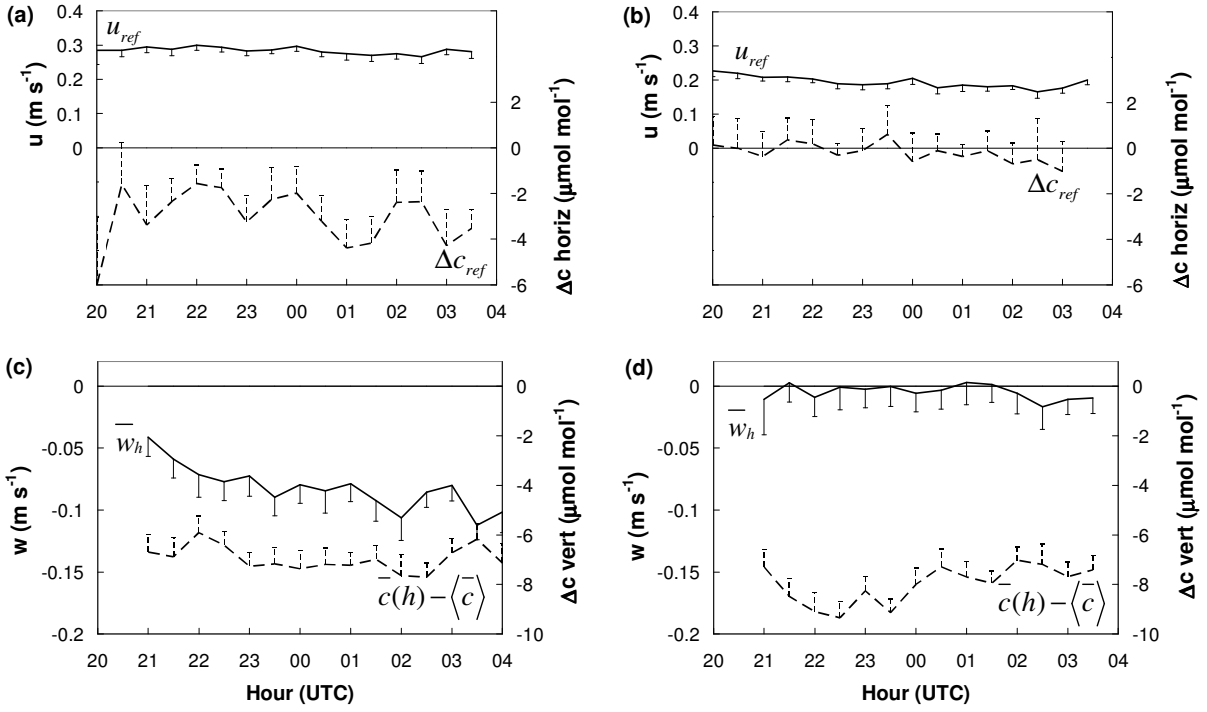

Fig. 10. Mean nocturnal evolution of **(a)** and **(b)** the horizontal wind component at the reference level (solid line), the horizontal [CO_2] difference at the reference level (dash line); **(c)** and **(d)** the ambient vertical wind component (solid line), the vertical [CO_2] difference (dash line). Established for periods with gravitational flows in the trunk space and above-wind direction from the NE sector (a and c) or the SW sector (b and d). Error bars represent standard error of the mean.

confirming that the aerodynamic method based on eddy covariance and storage measurements almost always underestimates the biological flux.

Horizontal advection contribution is about half the sum F_C+F_S in the NE sector and is negative (i.e., the control volume acts as a sink). It is about zero in the SW sector. Conversely, vertical advection reaches unrealistically high values in the NE sector. It is worth noting, however, that the time evolution of vertical advection in the NE sector is complementary to that of F_C+F_S. The night-to-night flux variability is important since the standard error is 4.9 μmol m^{-2} s^{-1} for the NE sector and 2.8 μmol m^{-2} s^{-1} for the SW sector. It results mainly from $\bar{w}_h$ variability.

Finally, the nocturnal evolution of the sum of turbulent, storage and advection terms is presented for the two sectors in Fig. 11e and f. It is clear that, in vertical convergence situation, this sum greatly overestimates the *NEE*, giving unrealistic values compared with the expected ecosystem respiration. This result is very similar to that presented by Leuning et al. (personal communication) in an Australian eucalyptus forest where positive vertical advection dominated the nocturnal CO_2 balance, giving unrealistic values of respiration compared with independent measurements using chambers. In equilibrium situation, this sum is highly variable but it is clear that the inclusion of advection terms in the CO_2 budget does not offset the night flux underestimation in these conditions.

10 Discussion

The CO_2 budget including advective fluxes presented in Fig. 11 does not provide an acceptable estimation of the expected night-time respiration. The potential reasons for the discrepancies are now discussed.

When computing F_{HA}, we have neglected any horizontal CO_2 mean transport between the gravitational layer and the canopy top. This choice was mainly driven by technical limitations. There have been few studies on vertical F_{HA} profiles in forests under gravitational flows. Feigenwinter et al. (2004) showed that, in a spruce forest site (Tharandt, Germany), 70% of the total F_{HA} occurred between 0 and 0.4 h_c (with h_c being the canopy height). In another study, Feigenwinter et al. (2008), working on a mountain slope (Renon, Italy), showed that the percentage of total F_{HA} occurring between 0 and 0.5 h_c could be as high as 65%, despite a gravitational layer being thicker than the forest height. We thus expect that the major part of F_{HA} will take place in the

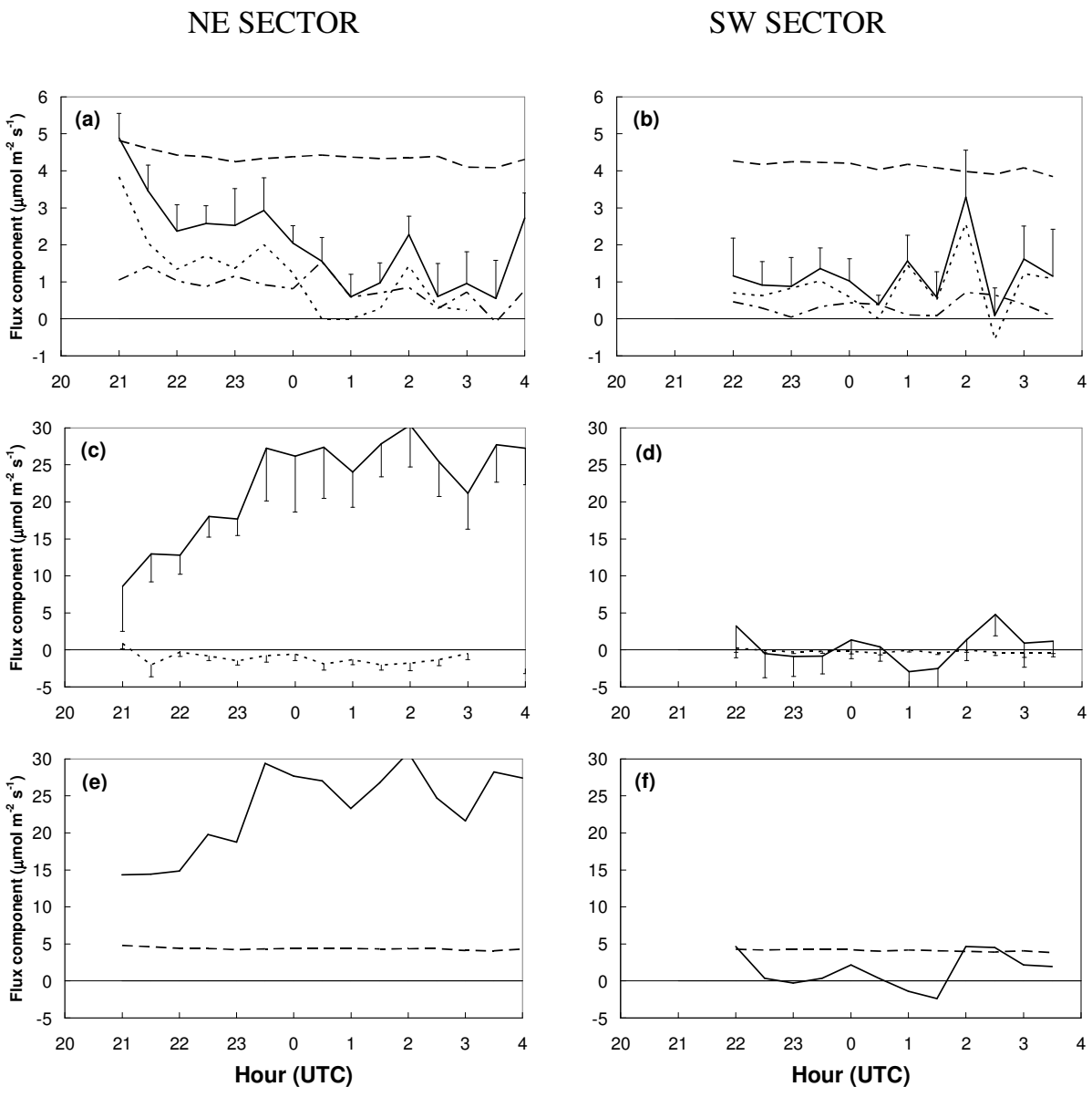

Fig. 11. Mean nocturnal evolution of turbulent flux (F_C), storage (F_S), *NEE*, horizontal advection (F_{HA}) and vertical advection (F_{VA}) for periods with gravitational flows in the trunk-space. Error bars represent standard error of the mean. a, c, e: above-wind direction from the NE sector. b, d, f: above-wind direction from the SW sector. **(a)** and **(b)**: F_C (dash-dotted line), F_S (dotted line), F_C+F_S (solid line) and NEE (dashed line). **(c)** and **(d)**: F_{HA} (dotted line), F_{VA} (solid line). **(e)** and **(f)**: $F_C+F_S+F_{HA}+F_{VA}$ (solid line) and NEE (dashed line).

gravitational layer but we cannot exclude the possibility of missing an important part of this transport.

In Heinesch et al. (2007), we already mentioned the difficulty of obtaining a reliable estimate of $\bar{w}_h$ and distinguishing the respective importance of the measurement uncertainty and the natural variability of this variable. An important F_{VA} night-to-night variability was also mentioned in all the publications proposing an evaluation of this term. Marcolla et al. (2005) obtained standard errors ranging between 1 and 2 μmol m^{-2} s^{-1} while the other studies underline the great dispersion of measurements (Baldocchi et al., 2000; Feigenwinter et al., 2004; Feigenwinter et al., 2008; Lee, 1998; Paw U et al., 2000 ; Staebler et Fitzjarrald, 2004; Sun et al., 2007).

Another source of uncertainty relates to the vertical velocity vertical profile shape. In this study, a linear shape was chosen. The assumption was proposed initially by Lee (1998) and considered by Finnigan (1999) to be realistic, based on theoretical considerations resulting from air flow modelling. However the model did not take into ac-

count the impact of the vegetation or thermal stratification. Very few experimental checks of this assumption appear in the literature because of the difficulty of measuring $\bar{w}$ in or below the canopy. Marcolla et al. (2005) measured a five-point vertical profile of $\bar{w}$ and concluded that the linearity assumption is rather well respected. However, this result was established for a relatively open and small forest. In addition, due to the greater and longer slope, the layer in which the gravitational flow was established was much thicker than at Vielsalm and included the totality of the vertical profile (no decoupling between above and below the canopy). This situation cannot thus be extrapolated to the Vielsalm site. In a more closed forest, Staebler (2005) measured a vertical profile of three points and did not find a well-defined form for the $\bar{w}$ profile. He concluded that the assumption of linearity can be neither validated nor invalidated by his measurements. Recently, Sun et al. (2007) made an arbitrary choice of a flat profile between a measurement level at 0.13 h_c and h_c (canopy height) connected to the ground with a linear decrease and to the measurement level at 1.9 h_c with a linear increase. This kind of assumption has an important quantitative impact on F_{VA} which should be investigated. We suspect that the linearity assumption was not correct at our site and that it is the main cause of F_{VA} overestimation in the convergence situation. This hypothesis is difficult to check as the planar fit method is impracticable in the canopy space because there are too many obstacles that inflect streamlines. However, we showed (Heinesch et al., 2007) that an alternative evaluation of $\bar{w}$ can be obtained from measurements of $\bar{u}$ horizontal divergence and application of the mass continuity equation. This gave a $\bar{w}$estimation at the gravitational layer top (20 m) that was four times lower than those inferred from the linear profile. If we take this estimate as an intermediate point associated with an arbitrarily chosen exponential profile, F_{VA} estimation based on this profile would be reduced by a factor of 4.1, compared with those based on the linear profile. For comparison, our computation suggests that the CO_2 balance closure in the NE sector (Fig. 11e) would require an F_{VA} reduction by a factor of 6.4. This suggests that the F_{VA} over-estimation found could result from the choice of an incorrect $\bar{w}$ profile shape. It's worth noting, however, that this explanation does not explain the lack of closure in the equilibrium situation.

11 Conclusions

It has been shown that the gravitational flows are linked with the vertical velocities above the canopy and that vertical flow convergence is associated with [CO_2] reduction along the streamlines while equilibrium is associated with a small [CO_2] enrichment along the streamlines. The coherence between measurements in stable atmospheric conditions of vertical wind speed at the top of cover, horizontal wind speed in the trunk space and horizontal [CO_2] profiles is all the more remarkable because these three variables are obtained by completely independent and particularly delicate measurements. It shows that, in spite of the inaccuracy affecting each measurement, these variables produce a coherent picture, suggesting that they reflect a real and repeatable phenomenon. The complete qualitative analysis of these advective terms would require knowing the CO_2 source distribution upstream, information not available in this study. This analysis fits the typology of advective transport proposed by Aubinet (in press) well. However, Vielsalm was presented in this typology as a convergence situation with positive F_{VA} and negative F_{HA}. We showed here that this conclusion should be balanced; a given site can present several distinct types of advective transport, even after having isolated nocturnal gravitational flow events. In the absence of modelling tools able to handle the complexity of these particular atmospheric conditions and site characteristics, we think that the proposed mechanisms, even if oversimplified, can be useful in the understanding of CO_2 transport in presence of gravitational flows.

However, despite their coherence, the same measurements did not allow nocturnal CO_2 balance closure because they produced unrealistic advection estimates. We suggest that one of the problems lies in an unrealistic hypothesis of $\overline{w}$ linear vertical profile. The tilt correction method being inapplicable in a closed canopy, the only alternative method available for estimating the $\overline{w}$ vertical profile is provided by the use of mass continuity. This technique, applied here with a basic 2-D experimental setup gives us indices that the $\overline{w}$ reduction with decreasing height is more important than postulated leading to a strongly reduced vertical advection.

We conclude that direct CO_2 advection estimations, even if not accurate enough to discuss the CO_2 balance of the site, can be used to detect events when the mean flow is advecting CO_2. This, at least, provides a physical justification for applying the u_* correction to these events and should be used to improve the filtering approach, especially at sites where the u_* correction is difficult to apply.

Acknowledgements. This research was supported by the European Commission's Environment and Climate Programme, CarboEurope project, under contract GOCE-CT2003-505572. The team was supported by the Fonds National de la Recherche Scientifique in Belgium.

Edited by: E. Falge

References

Aubinet, M.: Eddy-covariance CO_2 flux measurements in nocturnal conditions: an analysis of the problem, Ecological Applications, in press, 2008.

Aubinet, M., Berbigier, P., Bernhofer, C., Cescatti, A., Feigenwinter, C., Granier, A., Grunwald, T., Havrankova, K., Heinesch, B., Longdoz, B., Marcolla, B., Montagnani, L., and Sedlak, P.: Comparing CO_2 storage and advection conditions at night at different

CARBOEUROFLUX sites, Boundary-Layer Meteorology, 116, 63–94, 2005.

Aubinet, M., Chermanne, B., Vandenhaute, M., Longdoz, B., Yernaux, M. and Laitat, E.: Long term carbon dioxide exchange above a mixed forest in the Belgian Ardennes, Agricultural and Forest Meteorology, 108, 293–315, 2001.

Aubinet, M., Grelle, A., Ibrom, A., Rannik, Ü., Moncrieff, J., Foken, T., Kowalski, A. S., Martin, P. H., Berbigier, P., Bernhofer, C., Clement, R., Elbers, J., Granier, A., Grünwald, T., Morgenstern, K., Pilegaard, K., Rebmann, C., Snijders, W., Valentini, R. and Vesala, T.: Estimates of the annual net carbon and water exchange of forests: the EUROFLUX methodology, Adv. Ecol. Res., 30, 113–175, 2000.

Aubinet, M., Heinesch, B., and Yernaux, M.: 'Horizontal and vertical CO_2 advection in a sloping forest', Boundary-Layer Meteorology. 108, 397-417, 2003

Baldocchi, D. D., Hicks, B. B., and Meyers, T. P.: Measuring biosphere-atmosphere exchanges of biologically related gases with micrometeorological methods, Ecology, 69, 1331–1340, 1988.

Baldocchi, D. D., Finnigan, J., Wilson, K., Paw U, K. T., and Falge, E.: On measuring net ecosystem carbon exchange over tall vegetation on complex terrain, Bound.-Lay. Meteorol., 96, 257–291, 2000.

Feigenwinter, C., Bernhofer, C., Eichelmann, U., Heinesch, B., Hertel, M., Janous, D., Kolle, O., Lagergren, F., Lindroth, A., Minerbi, S., Moderow, U., Mölder, M., Montagnani, L., Queck, R., Rebmann, C., Vestin, P., Yernaux, M., Zeri, M., Ziegler, W., and Aubinet, M.: Comparison of horizontal and vertical advective CO_2 fluxes at three forest sites, Agricultural and Forest Meteorology., 148, 12–24, 2008.

Feigenwinter, C., Bernhofer, C., and Vogt, R.: The influence of advection on the short term CO_2 budget in and above a forest canopy, Bound.-Lay. Meteorol., 113, 201–224, 2004.

Finnigan, J. J.: A comment on the paper by Lee (1998): On micrometeorological observations of surface-air exchange over tall vegetation, Agricultural and Forest Meteorology, 97, 55–64, 1999.

Froelich, N. J., Schmid, H. P., Grimmond, C. S. B., Su, H. B., and Oliphant, A. J.: Flow divergence and density flows above and below a deciduous forest. Part I. Non-zero mean vertical wind above canopy, Agricultural and Forest Meteorology., 133, 140–152, 2005.

Goulden, M. L., Miller, S. D., and da Rocha, H. R.: Nocturnal cold air drainage and pooling in a tropical forest', J. Geophys. Res.-Atmos., 111, D08S04, doi:10.1029/2005JD006037, 2006.

Gu, L. H., Falge, E. M., Boden, T., Baldocchi, D. D., Black, T. A., Saleska, S. R., Suni, T., Verma, S. B., Vesala, T., Wofsy, S. C., and Xu, L. K.: Objective threshold determination for nighttime eddy flux filtering', Agricultural and Forest Meteorology, 128, 179–197, 2005.

Heinesch, B., Yernaux, M., and Aubinet, M.: Some methodological questions concerning advection measurements: a case study, Bound.-Lay. Meteorol., 122, 457–478, 2007

Knohl, A., Schulze, E. D., Kolle, O., and Buchmann, N.: Large carbon uptake by an unmanaged 250-year-old deciduous forest in Central Germany, Agricultural and Forest Meteorology. 118, 151–167, 2003

Laitat, E., Chermanne, B., and Portier, B.: Biomass, carbon and nitrogen allocation in open top chambers under ambient and elevated CO_2 and in a mixed forest stand. A tentative approach for scaling up from the experiments of Vielsalm in Forest Ecosystem Modelling, Upscaling and Remote Sensing. Academic Publishing, The Hague, The Netherlands, 33–60, 1999.

Lee, X.: On micrometeorological observations of surface-air exchange over tall vegetation, Agricultural and Forest Meteorology. 91, 39–49, 1998.

Lee, X., Massman, W. J., and Law, B.: Handbook of Micrometeorology : A Guide for Surface Flux Measurement and Analysis, Kluwer Academic Publishers, Dordrecht, The Netherlands, 250, 2004.

Loescher, H. W., Law, B. E., Mahrt, L., Hollinger, D. Y., Campbell, J., and Wofsy, S. C.: Uncertainties in, and interpretation of, carbon flux estimates using the eddy covariance technique, J. Geophys. Res.-Atmos., 111, D21S90, doi:10.1029/2005JD006932, 2006.

Mahrt, L.: Momentum balance of gravity flows, J. Atmos. Sci., 39, 2701–2711, 1982.

Marcolla, B., Cescatti, A., Montagnani, L., Manca, G., Kerschbaumer, G., and Minerbi, S.: Role of advective fluxes in the carbon balance of an alpine coniferous forest, Agricultural and Forest Meteorology., 130, 193–206, 2005.

Paw U, K. T., Baldocchi, D. D., Meyers, T. P., and Wilson, K. B.: Correction of eddy-covariance measurements incorporating both advective effects and density fluxes, Bound.-Lay. Meteorol., 97, 487–511, 2000

Staebler, R. M., and Fitzjarrald, D. R.: Observing subcanopy CO_2 advection, Agricultural and Forest Meteorology., 122, 139–156, 2004.

Staebler, R. M., and Fitzjarrald, D. R.: Measuring canopy structure and the kinematics of subcanopy flows in two forests, J. Appl. Meteorol., 44, 1161–1179, 2005

Stull, R. B.: An introduction to Boundary Layer Meteorology, Kluwer Academic Publishers, Dordrecht, 666p., 1988.

Sun, J., Burns, S. P., Delany, A. C., Oncley, S. P., Turnipseed, A., Stephens, B. B., Lenschow, D. H., Lemone, M. A., Monson, R. K., and Anderson, D.: CO_2 transport over complex terrain, Agricultural and Forest Meteorology. 145, 1–21, 2007.

Van Gorsel, E., Leuning, R., Cleugh, H. A., Keith, H., and Suni, T.: Nocturnal carbon efflux: reconciliation of eddy covariance and chamber measurements using an alternative to the u(*)-threshold filtering technique, Tellus Series B-Chemical and Physical Meteorology. 59, 397–403, 2007.

Yi, C. X., Monson, R. K., Zhai, Z. Q., Anderson, D. E., Lamb, B., Allwine, G., Turnipseed, A. A., and Burns, S. P.: 'Modeling and measuring the nocturnal drainage flow in a high-elevation, subalpine forest with complex terrain', J. Geophys. Res.-Atmos., 110, D22303, doi:10.1029/2005JD006282, 2005.